Carbon geochemistry of plankton-dominated samples in the Laptev and East Siberian shelves: contrasts in suspended particle composition

Tesi Tommaso [1,2,3], Marc C. Geibel [1,2], Christof Pearce [2,4,5], Elena Panova [6], Jorien E. Vonk [7], Emma Karlsson[1,2], Joan A. Salvado[1,2], Martin Krusâ[1,2], Lisa Bröder [1,2], Christoph Humborg [1,2], Igor Semiletov[6,8,9], Örjan Gustafsson [1,2]

[1] Department of Environmental Science and Analytical Chemistry (ACES), Stockholm University

[2] Bolin Centre for Climate Research, Stockholm University

[3] Institute of Marine Sciences, National Research Council (ISMAR-CNR)

[4] Department of Geological Sciences, Stockholm University, Sweden

[5] Department of Geoscience, Aarhus University, Denmark

[6] Tomsk Polytechnic University

[7] Vrije Universiteit Amsterdam (VU)

[8] Pacific Oceanological Institute FEB RAS

[9] University of Alaska Fairbanks

Abstract

Recent Arctic studies suggest that sea-ice decline and permafrost thawing will affect phytoplankton dynamics and stimulate heterotrophic communities. However, in what way the plankton composition will change as the warming proceeds remains elusive. Here we investigate the chemical signature of the plankton-dominated fraction of particulate organic matter (POM, >10μm) collected along the Siberian shelf. POM (>10μm) samples were analysed using molecular biomarkers (CuO oxidation and IP_{25}) and dual-carbon isotopes ($\delta^{13}C$ and $\Delta^{14}C$). In addition, surface water chemical properties were integrated with the POM (>10μm) dataset to understand the link between plankton composition and environmental conditions.

$\delta^{13}C$ and $\Delta^{14}C$ exhibited a large variability in the POM (>10μm) distribution while terrestrial biomarkers showed a negligible input from terrestrial sources. In the Laptev Sea (LS) open-waters, $\delta^{13}C$ and $\Delta^{14}C$ fingerprint of POM (>10μm) suggested that dissolved organic carbon (DOC) from the Lena river was the primary source of metabolizable carbon indicating, thus, a heterotrophic environment. Moving eastwards toward the sea-ice dominated East Siberian Sea (ESS), the system became progressively more autotrophic. Comparison between $\delta^{13}C$ of POM (>10μm) samples and CO_2aq concentrations revealed that the carbon isotope fractionation increased moving toward the easternmost and most productive stations.

In a warming scenario characterized by enhanced terrestrial DOC release (thawing permafrost) and progressive sea-ice decline, heterotrophic conditions might persist in the LS while the nutrient-rich Pacific inflow will likely stimulate greater ESS primary productivity in the ESS. The contrasting trophic conditions will result in a sharp gradient in $\delta^{13}C$ between the LS and ESS similar to what documented in our semi-synoptic study.

1. Introduction

The progressive reduction of sea-ice extent in the Arctic Ocean is indisputable evidence of modern global warming (Comiso et al., 2008; Ding et al., 2017; Kwok and Rothrock, 2009). The unprecedented decline of sea-ice is expected to alter several aspects of the Arctic marine ecology such as plankton abundance and its temporal distribution (Arrigo et al., 2008). For instance, recent studies suggest that the increase of solar irradiance will stimulate greater primary productivity in summer while the prolonged ice-free conditions will develop a second algal bloom in early fall, which is a distinctive feature of only lower latitudes (Ardyna et al., 2014; Lalande et al., 2009; Lalande et al., 2014). The phytoplankton communities are expected to profoundly change towards a higher contribution from open water phytoplankton at the expense of sea-ice assemblages (Fujiwara et al., 2014). Taken together, a greater productivity in the ice-free or marginal ice zone compare to the multi-year ice system, is also expected to lead to greater carbon uptake and settling export of organic carbon from the surface to deeper strata of the Arctic Ocean (Gustafsson and Andersson, 2012).

Sea-ice decline will also affect the water-air gas exchange, currents and river plume dispersion which, in turn, exert large control on the surface water chemical/physical properties (Aagaard and Carmack, 1989; Ardyna et al., 2014; Lalande et al., 2014). On top of this, destabilization of permafrost soils and the terrestrial cryosphere will result in enhanced particulate and dissolved carbon input to the Arctic Ocean (Frey and Smith, 2005; Vonk et al., 2012). As a result, the geochemical signature of both autotrophic and heterotrophic plankton communities is also expected to change as the warming proceeds. However, how the warming will ultimately affect the marine geochemical signal is poorly understood. This study seeks a better understanding of the chemical composition of plankton that dominates regions of the Arctic Ocean characterized by different sea-ice coverages, nutrient availability and riverine

influence. In particular, we focus on the carbon isotope fingerprint (i.e. $\delta^{13}C$ and $\Delta^{14}C$) of plankton that grows in ice-covered and ice-free Marginal Ice Zone (MIZ) regimes on the Siberian margin. The motivation behind investigating the chemical fingerprint of plankton from different regimes is to provide a better understanding of the carbon signature for direct applications to carbon studies of both modern systems and paleo-reconstructions. In particular, the isotope composition of marine OC finds several applications in climate, ecology and carbon source apportionment studies. For example, stable carbon isotopes of marine phytoplankton are used for paleo-pCO_2 reconstructions over geological time scales (Hoins et al., 2015; Pagani et al., 1999; Popp et al., 1999; Rau, 1994). The $\delta^{13}C$ signature also provides a solid tool for marine food web and ecosystem structure investigations (Dunton et al., 2006; Iken et al., 2005; Kohlbach et al., 2016). Furthermore, dual-carbon isotope mixing models ($\delta^{13}C$ and $\Delta^{14}C$) are commonly used to quantify the relative proportion of marine and various allochtonous sources (e.g., permafrost soil) in both contemporary and paleo-reconstructed carbon cycling of the Arctic (Karlsson et al., 2016; Tesi et al., 2016; Vonk et al., 2012; Vonk et al., 2014).

With this overarching goal in mind, here we investigate the >10 μm fraction of particulate organic matter (POM) in ice-covered and ice-free MIZ regimes of the Siberian Arctic Shelf during the SWERUS-C3 expedition (July-August 2014) (Fig. 1). The plankton-dominated POM samples collected throughout the ca. 4,500 km long cruise track were characterized using bulk parameters (OC, $\delta^{13}C$ and $\Delta^{14}C$) and biomarkers (highly branched isoprenoids, IP_{25}; CuO oxidation products). In addition, continuous measurements of dissolved CO_2 (CO_{2aq}) and its stable carbon isotope composition ($\delta^{13}C_{CO2}$) were performed during the campaign (Humborg et al., 2017) and used for a direct comparison with the chemical composition of the POM fraction.

2. Study region

The Laptev Sea and the East Siberian Sea are shallow epicontinental seas in the Russian Arctic separated by the New Siberian Islands (Fig. 1). Sea-ice cover lasts for most part of the year over the shelf. Late spring/summer is characterized by the seasonal sea-ice retreat coupled with river freshet which supplies large amount of terrestrial carbon in the form of particulate and dissolved matters (Karlsson et al., 2016; Salvadó et al., 2016; Sánchez-García et al., 2011). The Lena (523 km3/y), Indigirka (54 km3/y), and Kolyma (48 km3/y) are the major rivers (Gordeev, 2006). During the ice-free season, the Lena plume can be traced in the outer-shelf of the Laptev Sea (Fichot et al., 2013; Salvadó et al., 2016; Sánchez-García et al., 2011) while Pacific inflow from the Bering strait affects further east the East Siberia margin (Semiletov et al., 2005). The Pacific inflow exerts control on the nutrient balance as it supplies nitrates and nitrites to an otherwise nutrient-depleted region (Anderson et al., 2011; Semiletov et al., 2005). Another important source of particulate material to the continental margin is the Pleistocene Ice Complex Deposit (ICD) entering the ocean via coastal erosion (Lantuit et al., 2011; Vonk et al., 2012) which is the dominant carbon source between the Kolyma river and the Lena river (Vonk et al., 2012).

3. Methods

3.1 POM (<10 μm) sampling

Seawater was pumped from a stainless steel inlet on the hull of the icebreaker *Oden* positioned at 8 m below the sea surface. The inlet system is tested and further described in Sobek and Gustafsson (2004) and Gustafsson et al. (2005). Figure 1a and 1b show the regions covered to harvest each POM (>10 μm) sample with their location shown as time-averaged position. The particulate material was retained via a large volume filtration apparatus using a 10-μm Nitex® (nylon) mesh placed in a 29.3 cm filter holder. After collection, filtered

particulate material was transferred in pre-clean HDPE tubes by rinsing the Nitex® filters with MilliQ water. Samples were kept frozen throughout the expedition. In the lab, samples were transferred in pre-cleaned Falcon® tubes (rinsed with 0.1M HCl) and gently centrifuged to remove the supernatant. The residual particulate material was frozen and subsequently freeze-dried prior to biogeochemical analyses.

3.2 Bulk carbon isotopes and biomarker analyses

Organic carbon (OC) and stable carbon isotope ($\delta^{13}C$) analyses were carried out on acidified samples (Ag capsules, HCl, 1.5M) to remove the carbonate fraction (Nieuwenhuize et al., 1994). Analyses were performed using a Thermo Electron mass spectrometer directly coupled to a Carlo Erba NC2500 Elemental Analyzer via a Conflo III (Department of Geological Sciences, Stockholm University). OC values are reported as weight percent (%d.w.) whereas stable isotope data are reported in the conventional $\delta^{13}C$ notation (‰). The analytical error for $\delta^{13}C$ was lower than ±0.1‰ based on replicates. Acidified (HCl, 1.5 M) samples for radiocarbon abundance were analysed at the US-NSF National Ocean Science Accelerator Mass Spectrometry (NOSAMS) facility (Woods Hole Oceanographic Institution, Woods Hole, USA). Radiocarbon data are reported in the standard $\Delta^{14}C$ notation (‰).

Alkaline CuO oxidations were carried out using an UltraWAVE Milestone microwave as described in Tesi et al. (2014). Briefly, about 2 mg of OC was oxidised using CuO under alkaline (2N NaOH) and oxygen-free conditions at 150 °C for 90 min in teflon tubes. After the oxidation, known amounts of recovery standards (trans-cinnamic acid and ethylvanillin) were added to the solution. The NaOH solutions were then acidified to pH 1 with concentrated HCl and extracted with ethyl acetate. Extracts were dried and redissolved in pyridine. CuO oxidation products were quantified by GC-MS in full scan mode (50-650 m/z). Before GC analyses, the CuO oxidation products were derivatized with bis(trimethylsilyl)

trifluoroacetamide+1% trimethylchlorosilane at 60°C for 30 min. The compounds were separated chromatographically in a 30m×250 µm DB5ms (0.25 µm thick film) capillary GC column, using an initial temperature of 100°C, a temperature ramp of 4°C/min and a final temperature of 300°C. Lignin phenols (terrestrial biomarkers) were quantified using the response factors of commercially available standards (Sigma-Aldrich) whereas the rest of the CuO oxidation products were quantified by comparing the response factor of trans-cinnamic acid. Lignin-derived reaction products include vanillyl phenols (V=vanillin, acetovanillone, vanillic acid), syringyl phenols (S=syringealdehyde, acetosyringone, syringic acid) and cinnamyl phenols (C=p-coumaric acid, ferulic acid). In addition to lignin, cutin-derived products (hydroxyl fatty acids) were used to trace the land-derived input (Goñi and Hedges, 1990; Tesi et al., 2010). Other CuO oxidation products include para-hydroxybenzene monomers (P-series), benzoic acids (B-series) and short-chain fatty acids (FA-series) which can have both terrestrial and marine origin (Goñi and Hedges, 1995; Tesi et al., 2010).

The sea-ice proxy IP_{25} (mono-unsaturated highly branched isoprenoid (HBI) alkene) was quantified according to Belt et al. (2012). IP_{25} producers are a minor (<5%) fraction of the total sea-ice taxa which are, however, ubiquitous in pan-Arctic sea-ice. Species include *Pleurosigma stuxbergii var. rhomboide*, *Haslea crucigeroides* (and/or *Haslea spicula*) and *Haslea kjellmanii* (Brown et al., 2014a). Briefly, lipids were extracted via sonication using a dichloromethane/methanol solution (2:1 v/v × 3). Prior to the extraction, two internal standards (7-hexylnonadecane, 7-HND and 9- octylheptadecene, 9-OHD) were added to permit quantification of IP_{25} (monounsaturated highly branched isoprenoid) following analysis via GC-MS. Total lipid extracts (TLEs) were dried under N_2 after removing the water excess with anhydrous $NaSO_4$. Dry TLEs were redissolved in dichloromethane and the non-polar hydrocarbon fraction was purified using open column chromatography (deactivated

175 SiO_2) and hexane as eluent. Saturated and unsaturated n-alkanes were further separated using
176 10% $AgNO_3$ coated silica gel using hexane and dichloromethane, respectively.

177 Quantification of IP_{25} was carried out in SIM mode (*m/z* 350.3) as described in Belt et
178 al. (2012). The GC was fitted with a 30m×250 µm DB5ms (0.25 µm thick film) capillary GC
179 column. Initial GC oven temperature was set to 60°C followed by a 10°C/min ramp until a
180 final temperature of 310°C (hold time 10 min).

181

182 **3.3. Microscope images of plankton**

183 High resolution digital images were taken with an Environmental Scanning Electron
184 Microscope (ESEM) Philips XL30 FEG in high voltage (15kV) and magnification 250X.
185 Samples were further studied for identification of diatoms and dinoflagellates using a
186 transmitted light microscope (Leitz Laborlux 12 Pol) equipped with differential interference
187 contrast optics at 1000X magnification. Microscope slides were prepared using settling
188 chambers to achieve an even distribution of particles on the cover glass, regardless of size and
189 shape Warnock and Sherer (2014).

190 **3.4 Sea-ice data**

191 Daily AMSR2 sea-ice extent and concentration maps were provided by the Institute of
192 Environmental Physics, University of Bremen, Germany (Spreen et al., 2008) as GeoTIFF
193 files (ftp://seaice.uni-bremen.de).

194

195 **3.5 Statistics**We used two-tailed T-test (homoscedasticity) and Welch T-test
196 (heteroskedasticity) to assess whether the differences between open waters and sea-ice
197 dominated waters were statistically significant. For this study, significance level (alpha) was
198 set at 0.01.

199

4. Surface water conditions during the SWERUS-C3 expedition

Before discussing the chemical composition of the POM (>10 μm), here we briefly introduce the different environmental conditions encountered throughout the cruise track. The surface water data presented in this section were pulled together from previous studies which provide an in-depth analysis of the surface water properties during the SWERUS-C3 expedition in 2014 (Humborg et al., 2017; Salvadó et al., 2016) (Table 2). For this study, continuous CO_2aq and $\delta^{13}C_{CO2}$ data (Humborg et al., 2017) were averaged to match the water sampling stations allowing for a direct comparison with DOC and salinity data (Fig. 2) (Supplementary Material).

Summer 2014 was consistent with the long-term downward trend in Arctic sea-ice extent. The strongest anomalies were observed in the LS which experienced the most northerly sea-ice shift since satellite observations began in 1979 (National Snow and Sea Ice Data Center, NSIDC. http://nsidc.org/data). Unpublished data). In general, sea-ice displayed a strong gradient over the study region going from ice-free conditions in the outer LS to ice-dominated waters in the outer ESS (Fig.1.) Three snapshots of the sea-ice extent and concentrations (.i.e. at the beginning, in the middle and at the end of the sampling) is shown in Fig.1. Furthermore, Table 1 reports the averaged sea-ice concentrations encountered during the collection of each sample.

The surface water salinity exhibited a longitudinal trend characterized by low values in the outer LS while the sea-ice dominated ESS waters showed relatively higher values (Fig. 2a; Table 2). However, the highest salinity values were measured in the westernmost stations resulting in a sharp gradient in the LS. The low surface water salinities in the outer LS are most likely the result of both Lena river input and sea-ice thawing (Humborg et al., 2017) that started in late May (Janout et al., 2016).

The highest DOC concentrations were measured in the mid-outer LS in the surface water plume affected by Lena River runoff (Fig.2b; Table 2). Overall, DOC concentrations followed the plume dispersion with high DOC concentrations corresponding to low salinities (Fig. 2). Carbon stable isotopes ($\delta^{13}C$) and terrestrial biomarkers (of the solid-phase extracted DOC fraction; Salvado et al., 2016) further confirmed the influence of terrestrial DOC in the outer LS, while the land-derived input progressively decreased moving eastward.

CO_2aq concentrations exhibited a typical estuarine pattern over the study region (Humborg et al., 2017) (Fig. 2d; Table 2). Low salinity waters in the outer LS showed above atmospheric CO_2 concentrations (i.e., oversaturation) while surface waters below sea-ice exhibited undersaturated concentrations. The most depleted $\delta^{13}C_{CO2}$ values were measured off the Lena river mouth (Fig. 2e; Table 2). Being relatively rich in land-derived material, it is likely that respired terrestrial OC within the Lena river plume exerted control on the CO_2 isotopic signature and concentration (Humborg et al., 2017).

Finally, nutrient distribution revealed nitrate (NO_3) and nitrite (NO_2) depletion in surface waters throughout the cruise track (Humborg et al., 2017) in comparison with the Arctic Ocean gateways such as the Bering strait. Here, nutrient concentrations in surface waters are two-order of magnitude higher compared the our study region (Torres-Valdés et al., 2013). Phosphate (PO_4) exhibited rather low concentrations in the outer LS and relatively higher concentrations below the sea-ice in the outer ESS (Humborg et al., 2017) likely reflecting the inflow of nutrient-rich Pacific waters (Anderson et al., 2011; Semiletov et al., 2005; Torres-Valdés et al., 2013).

5. Results and discussion

5.1 Source of the POM (>10 μm) fraction

The Arctic Ocean off northern Siberia receives large quantities of dissolved and particulate terrestrial organic carbon via continental runoff and coastal erosion (Alling et al., 2010; Dittmar and Kattner, 2003; McClelland et al., 2016; Sánchez-García et al., 2011; Semiletov et al., 2013; Vonk et al., 2012). The land-derived material that does not settle in the coastal zone further travels across the continental margin reaching out to the outer-shelf region resuspended within the benthic nepheloid layer or in suspension within the surface river plume (Fichot et al., 2013; Sánchez-García et al., 2011; Wegner et al., 2003). Another fraction of terrestrial material can travel across the Siberian margin trapped in fast ice (Dethleff, 2005). Considering the potential allochthonous contribution, we addressed to what extent terrestrial organic material affects the POM (>10μm) fraction by quantifying the concentration of lignin phenols and C16-18 hydroxy fatty acids (cutin-derived products). These biomarkers are exclusively formed by terrestrial vegetation and, thus, serve as tracers of land-derived material in the marine environment (Amon et al., 2012; Bröder et al., 2016b; Feng et al., 2015).

Upon CuO alkaline oxidation the POM (>10μm) samples yielded only traces of lignin phenols while the cutin-derived products were not detected (Fig. 3). Other oxidation products in high abundance included saturated and mono-unsaturated short chain fatty acids (C12-18FA), para-hydroxy phenols, benzoic acids and dicarboxylic acids. These other reaction products are ubiquitous in both marine and terrestrial environments but they are predominant in plankton-derived material, especially short-chain fatty acids (Goñi and Hedges, 1995). When compared with active-layer permafrost soils and ice-complex deposits (Tesi et al., 2014), POM (>10μm) samples displayed a distinct CuO fingerprint dominated by short chain fatty acids (Fig. 3), consistent with the typical CuO products yields by phytoplankton batch cultures upon CuO alkaline oxidation (Goñi and Hedges, 1995). SEM images further

corroborated the abundance of marine plankton detritus in the POM (>10μm) fraction while lithogenic particles (clastic material) appeared to be sporadic in all samples.

The OC content (% d.w.) of the POM (>10um) fraction decreased eastwards showing high concentrations in the LS and relatively low values in the ESS (Table 1; $p<0.01$ T-test). However, in terms of absolute concentration in the water column (μC/l), the highest levels were generally observed in the sea-ice covered region (Table 1; Fig. 4a; $p<0.01$ T-test). Qualitative analyses by SEM and transmitted-light microscopy highlight important differences in plankton assemblages which reflect different timing of the plankton blooms which can explain these differences in concentration. Specifically, the open-water LS stations exhibited a low degree of plankton diversity and were largely dominated by a bloom of heterotrophic dinoflagellate cysts (*Protoperidinium* spp) (Fig. 5a; Table 3). Moving towards the ice-dominated regions, diatoms become the prevailing species. Dominant diatom genera include *Chaetoceros spp.* (dominant diatom in several stations), *Thalassiosira spp.*, *Rhizosolenia spp.*, *Coscinodiscus spp.*, *Asteromphalus spp.*, *Navicula spp.* as well as sea-ice species such as *Fragilariopsis cylindrus* and *Fragilariopsis oceanica* (Fig. 5b,c; Table 3).

Moored optical sensors deployed in the LS shelf recorded the sea-ice retreat in 2014 and found no sign of pelagic under-ice blooms despite available nutrients while high chlorophyll concentrations were detected immediately after the ice retreated in late May (Janout et al., 2016). The ice-edge blooms lasted for about 2 weeks according to the high resolution chlorophyll time-series (Janout et al., 2016). Thus, our post-bloom sampling in the LS essentially captured an oligotrophic environment dominated by heterotrophic dinoflagellate cysts (i.e, Protoperidinium spp) which likely fed on phytodetritus and river-derived organic material. Such conditions are fairly consistent with the relatively low carbon contents (μgC/L) observed in LS waters (Fig. 4a).

297 The Arctic sea-ice biomarker IP25 (Fig. 4b) further highlight the different regimes
298 observed in ice-free and ice-dominated surface waters. IP25 is a proxy of sea-ice based on a
299 highly branched mono-unsaturated isoprenoid alkene found in some sea-ice diatoms which,
300 however, generally account for 5% of the total sea-ice taxa (Belt et al., 2007; Brown et al.,
301 2014b). The IP25 concentrations varied by several orders of magnitude over the study area
302 showing low concentrations in the open-water western region while the sea-ice dominated
303 surface waters to the east exhibited high concentrations especially at station 31b (Fig. 4b;
304 Table 1) ; $p<0.01$ Welch T-test). The fact that IP25 was still detectable throughout the ice-free
305 outer LS suggests that the proxy captured the signal of the sea-ice retreat that occurred shortly
306 before the sampling at the end of May/early June (Janout et al., 2016). Alternatively, the IP25
307 could have been advected from nearby sea-ice dominated regions.
308
309 **5.2. Dual carbon isotopes: $\delta^{13}C$ and $\Delta^{14}C$**
310 $\delta^{13}C$ and $\Delta^{14}C$ of the POM (>10μm) samples exhibited a distinctive longitudinal trend
311 across the study area between LS and ESS (Fig. 4c,d) ($p<0.01$ T-test) . Depleted $\delta^{13}C$ values
312 characterized the LS open waters ranging from -28.1 to -24.7‰ (Fig. 4c). Although within the
313 range of terrestrially-derived material, our CuO oxidation data (i.e. trace of lignin phenols and
314 absence of cutin-derived products) suggest that the "light" isotopic composition in the LS
315 might instead reflect the plankton assemblage dominated by heterotrophic dinoflagellate cysts
316 as previously described (e.g., *Protoperidinium* spp; Fig. 5a). More specifically, heterotrophic
317 dinoflagellates can adapt their metabolism depending on the substrate available (e.g., diatoms
318 and bacteria). Several studies have shown that terrestrial DOC greatly promotes bacteria
319 biomass production which in turn stimulates the growth of heterotrophic dinoflagellates
320 (Carlsson et al., 1995; Purina et al., 2004; Wikner and Andersson, 2012). Thus, in these
321 conditions, allochthonous terrestrial DOC is actively recycled by bacteria and transferred to

dinoflagellates which explains, thus, the depleted $\delta^{13}C$ values observed in the river-dominated samples (Carlsson et al., 1995).

The modern radiocarbon fingerprint of the Lena DOC discharge is consistent with $\Delta^{14}C$ signature of the POM (>10μm) fraction in the LS (up to +99 ‰), supporting the importance of terrestrial DOC as a carbon source for the food web in the river plume (Fig. 4d and 6). By contrast, comparison with other potential carbon sources which include the Lena river particulate organic carbon, surface sediments, Pleistocene coastal Ice-Complex Deposit and Pacific DIC inflow reveals a different (more depleted) radiocarbon fingerprint (Fig. 6). It is also import to highlight that the DOC within the Lena plume is one/two-order of magnitude higher than the particulate carbon pool supporting, thus, our hypothesis (Humborg et al., 2017; Salvadó et al., 2016).

Moving towards the ice-dominated ESS, surface waters progressively become more autotrophic and productive (Humborg et al., 2017) while the POM (>10μm) exhibited a wide $\delta^{13}C$ signature ranging from -28.6 to -21.2‰ (Fig. 4c). The most depleted values were observed across the transition zone between open-waters and sea-ice. Visual inspections of these samples revealed large abundance of the centric diatom *Chaetoceros* spp. (spores and vegetative cells; St22, Fig. 5b) while lignin and cutin data indicated, a negligible input of land-derived material. Primary factors determining the fractionation of stable carbon isotopes in phytoplankton are several and include CO_2aq concentration, $\delta^{13}Caq$, growth rate, cell size, cell shape, light and nutrient availability (Gervais and Riebesell, 2001; Laws et al., 1997a; Popp et al., 1998; Rau et al., 1996). Our understanding about isotopic fractionation has been historically achieved via laboratory experiments designed to test each factor under controlled conditions. In natural environments, however, different factors can compete with each other, sometimes in opposite directions. Yet, the existing knowledge about surface water properties

346 during the expedition (Humborg et al., 2017) can provide important constraints for the
347 isotopic signal interpretation.

348 For example, comparison with continuous $\delta^{13}C$-CO_2aq and CO_2aq data measured
349 throughout the cruise track - time-averaged to match the large volume filtration along the
350 cruise track (Table 1) - suggested a negligible role exerted by $\delta^{13}C$-CO_2aq (Fig. 7b) while
351 CO_2aq concentration correlated with the $\delta^{13}C$ of the POM (>10μm) fraction (r^2=0.72; p<0.01)
352 (Fig. 7a). Such a relationship fits with the general model according to which a low demand
353 (i.e., low growth rate) and high supply (i.e., abundant CO_2aq) favour high fractionation and
354 vice versa (Laws et al., 1997b; Laws et al., 1995; Wolf-Gladrow et al., 1999).

355 During the expedition, surface water properties (i.e. O_2 and CO_2, Table 2) (Humborg
356 et al., 2017) suggest that the productivity in the outer ESS increases moving eastward, as
357 commonly observed, likely due to the Pacific inflow (Björk et al., 2011; Semiletov et al.,
358 2005). As a result, the wide range of plankton $\delta^{13}C$ over the ESS can be explained in terms of
359 two different regimes: (a) in the transition zone between open waters and sea-ice, the
360 productivity was low but CO_2aq was oversaturated while (b) in the easternmost ESS,
361 productivity was high but CO_2aq was depleted (Fig. 7b). The former regime favours
362 fractionation while the latter does not (Fig. 7b). Different diatom assemblages can also be
363 another factor to consider although the phytoplankton diversity observed over ESS can be
364 considered rather small (e.g. *Chaetoceros spp.* dominant in most of the samples) compared to
365 the wide range of $\delta^{13}C$ observed (i.e., from -28.8 to -21.6) (Table 3).

366 The POM (>10μm) fraction in the sea-ice dominated ESS exhibited slightly - but
367 consistently - depleted $\Delta^{14}C$ values ranging from -62 to -49 ‰ (Fig. 4d). This region is
368 affected by the inflow of Pacific waters whose DIC exhibits, however, a modern $\Delta^{14}C$
369 signature (Griffith et al., 2012) (Fig. 6). By contrast, these results suggest the influence from
370 an aged carbon pool. As the ESS remains covered by sea-ice for most of the year, it is

possible that the sea-ice hampers the gas exchange with the atmosphere and acts as a lid by trapping CO_2 which derives from the breakdown of sedimentary organic material (Anderson et al., 2009; Semiletov et al., 2016), which might have such ages (Bröder et al., 2016a; Vonk et al., 2012). In these conditions, the pre-aged CO_2 accumulates underneath the sea-ice and is subsequently incorporated during carbon fixation by the phytoplankton. While oversaturated bottom waters were extensively documented in the region with important consequences on the local DIC (Anderson et al., 2009; Pipko et al., 2009), more work is clearly needed to understand if early diagenesis in sediments can also affect the radiocarbon signature of the CO_2aq underneath the sea-ice. Alternatively, the slightly depleted radiocarbon signature might indicate the presence of pre-aged terrestrial organic carbon (Fig. 6) in the POM (>10μm) samples, not reflected in the lignin and cutin tracers (Fig. 3). However, it would then remain elusive why such an aged land-derived influence was not visible in the river-dominated LS waters while it affected the sea-ice dominated region.

Taken together, our results indicate that the dual-carbon isotope fingerprint is highly affected by the trophic conditions (heterotrophic *vs* autotrophic) as well as the extent of primary productivity. In a warming scenario characterized by sea-ice retreat (Arrigo et al., 2008; Comiso et al., 2008) and enhanced terrestrial input from land as result of hydrology and permafrost destabilization (Frey and Smith, 2005; Vonk et al., 2012), the geochemical composition of plankton will likely change as the warming proceeds.

6. Conclusions

Analyses of large-volume filtrations of plankton-dominated >10 μm particle samples revealed a high degree of heterogeneity in the dual carbon isotope signature ($\delta^{13}C$ and $\Delta^{14}C$) between ice-free waters (Laptev Sea) and the ice-covered region (East Siberian Sea).

Our results suggest a heterotrophic environment in the outer LS open waters where the $\delta^{13}C$ depleted river DOC is transferred to relatively higher trophic levels via microbial incorporation in the river plume. Moving eastwards towards the ice-dominated outer ESS, surface waters became progressively more autotrophic. Here, the isotopic fractionation appears to follow the phytoplankton growth *vs* CO_2 demand model according to which carbon fractionation decreases at high growth and low CO_2 concentrations. As a result, the transition between open-waters and sea-ice exhibited more depleted $\delta^{13}C$ values compared to the productive easternmost stations. Radiocarbon signatures were slightly depleted over the whole sea-ice dominated area. This raises the question whether the sea-ice hampers the gas exchange with the atmosphere and trap the CO_2 sourced from reactive sedimentary carbon pools.

In a warming scenario, it is likely that the oligotrophic ice-free LS will be dominated by heterotrophic metabolism fuelled by terrestrially-derived organic material (i.e., Lena input). In these conditions, the dual-carbon isotope signature of the heterotrophic plankton will essentially reflect the terrestrial fingerprint. In the ESS, which receives the inflow of the nutrient-rich Pacific waters, ice-free conditions will enhance light penetration. This in turn might further stimulate phytoplankton growth with important implications in terms of CO_2 depletion and resulting low isotope fractionation. Altogether, this will result in a sharp compositional gradient (e.g. $\delta^{13}C$) between LS and ESS similar to what captured in our semi-synoptic study.

Acknowledgements

We thank the *I/B Oden* crew and the Swedish Polar Research Secretariat staff. This study was supported by the Knut and Alice Wallenberg Foundation (KAW contract 2011.0027), the Swedish Research Council (VR contract 621-2007-4631 and 621-2013-5297), European Research Council (ERC-AdG CC-TOP project #695331 to Ö.G.). T. Tesi

additionally acknowledges EU financial support as Marie Curie fellow (contract no. PIEF-GA-2011-300259). J.A. Salvadó acknowledges EU financial support as a Marie Curie grant (contract no. FP7-PEOPLE-2012-IEF; project 328049). I. Semiletov acknowledges financial support from the Russian Government (grant No. 14, Z50.31.0012/03.19.2014) and the Russian Foundation for Basic Research (nos. 13-05-12028 and 13-05-12041), and E. Panova from the Russian Scientific Foundation (grant no. 15-17-20032). We thank the Arctic Great Rivers Observatory (NSF-1107774) for providing DOC and POC river data (www.arcticgreatrivers.org).

Table 1. Chemical composition of the POM (>10μm) fraction and continuous CO_2aq measurements*

ID	Time averaged latitude (N)	Time averaged longitude (E)	Mean sea-ice percentage (%)	POM (>10μm) concentration (mg/l)	OC (d.w.)	$\delta^{13}C$ (‰)	$\Delta^{14}C$ (‰)	IP25 (ng/gOC)	averege CO_2aq (ppm)*	average $\delta^{13}C$-CO_2aq (‰)*
ST4	81.68	105.96	98.4	6	18.2	-26.7	n.d.	n.d.	323	-10.9
ST5	80.47	114.07	98.7	15	42.6	-27.6	n.d.	n.d.	322	-11.0
ST6	78.86	125.22	82.2	1	51.7	-26.6	99	n.d.	325	-10.8
ST7	77.88	126.62	0.0	11	43.1	-25.7	n.d.	88	350	-10.7
ST8	77.16	127.32	0.0	17	30.9	-26.7	41	n.d.	391	-10.5
ST9	76.78	125.83	0.0	3	31.5	-27.9	30	48	385	-10.5
ST10	76.90	127.81	0.0	11	40.9	-24.7	n.d.	n.d.	349	-11.0
ST11	77.12	126.66	0.0	13	29.6	-28.1	27	13	428	-10.7
ST22	77.67	144.63	0.0	20	11.3	-28.8	n.d.	95	394	-11.0
ST23	76.43	147.53	0.0	6	7.6	-28.5	-50	n.d.	394	-11.2
ST24	76.42	149.84	34.4	19	11.9	-26.8	-62	368	374	-11.1
ST25	76.62	152.03	96.7	23	19.5	-25.7	-31	465	263	-10.8
ST26	76.14	157.85	96.2	109	30.8	-24.2	-30	217	316	-10.9
ST27	75.00	161.03	91.5	41	23.3	-23.0	n.d.	256	299	-11.1
ST28	74.63	161.98	86.3	28	15.5	-23.8	n.d.	n.d.	214	-11.3
ST29	73.61	169.72	79.3	31	14.7	-23.2	-50	518	184	-11.3
ST30	75.61	174.01	66.7	43	22.6	-27.0	n.d.	n.d.	304	-10.5
ST31A	75.85	174.41	75.6	30	10.9	-21.6	-62	1911	182	-10.6
ST31B	74.26	173.74	63.5	15	4.6	-23.3	n.d.	783	n.d.	n.d.
ST32	73.56	176.06	51.8	21	11.3	-24.5	-58	131	n.d.	n.d.
ST33	72.35	-175.14	0.0	20	15.5	-23.5	n.d.	473	n.d.	n.d.
ST34	73.28	-173.05	28.7	76	13.4	-21.6	-52	970	n.d.	n.d.
ST35	75.21	-172.05	53.9	24	14.3	-24.2	n.d.	268	n.d.	n.d.

n.d = not determined
*Humborg et al. (2017)

Table 2. Surface water (0-20 m) chemical and physical properties during the SWERUS-C3 expedition*

	Salinity	Temperature	DIC	DOC	POC	δ^{13}C-DIC	NO_2 - NO_3	PO_4	O_2
		ºC	µmol kg^{-1}	µmol kg^{-1}	µmol kg^{-1}	‰	µmol kg^{-1}	µmol kg^{-1}	µmol kg^{-1}
	median	**median**	**median**	**median**	**median**	**median**	**median**	**median**	**median**
Outer LS shelf (0-20 m)	32.87	3.84	2139	149.1	7.9	0.75	0.21	0.27	323.0
LS shelf break (0-20 m)	33.56	0.57	2114	91.5	10.1	1.10	0.26	0.15	364.9
Outer ESS shelf (0-20 m)	29.45	-1.33	1969	84.2	10.7	1.14	0.25	0.97	381.5
ESS shelf break (0-20 m)	28.23	-1.32	1979	73.7	4.6	1.47	0.11	0.59	394.1
	mean	**mean**	**mean**	**mean**	**mean**	**mean**	**mean**	**mean**	**mean**
Outer LS shelf (0-20 m)	31.17	3.40	2119	179.8	7.9	0.58	0.60	0.29	327.0
LS shelf break (0-20 m)	33.42	0.96	2111	97.5	10.0	1.10	0.61	0.16	358.1
Outer ESS shelf (0-20 m)	28.95	-0.05	1949	95.8	11.9	1.26	0.26	0.95	386.8
ESS shelf break (0-20 m)	28.27	-1.31	1975	72.0	4.6	1.49	0.12	0.60	397.0
	s.d.	**s.d.**	**s.d.**	**s.d.**	**s.d.**	**s.d.**	**s.d.**	**s.d.**	**s.d.**
Outer LS shelf (0-20 m)	3.22	2.38	89	66.3	1.7	0.50	0.91	0.11	14.6
LS shelf break (0-20 m)	0.70	2.07	23	21.2	1.7	0.11	0.74	0.06	22.5
Outer ESS shelf (0-20 m)	1.41	2.28	75	30.2	4.6	0.49	0.12	0.19	32.2
ESS shelf break (0-20 m)	0.53	0.04	49	3.2	0.3	0.08	0.03	0.02	8.3

*data from Humborg et al. (2017) and Salvadó et al. (2016)

Table 3. Qualitative plankton characterization of selected POM (>10μm) samples

ID	Region	Diatoms	Dinoflagellates	Other species
ST6	LS	Few *Coscinodiscus*	None observed	
ST9	LS	None observed	Few *Protoperidinium*	
ST11	LS	None observed	Abundant *Protoperidinium*	
ST22	LS-ESS	Abundant *Chaetoceros*, few *Rhizosolenia*, *Thalassiosira*	None observed	
ST25	LS-ESS	High diversity. Abundant *Chaetoceros, few Rhizosolenia, Coscinodiscus, Thallasiosira, Asteromphalus, Navicula*	None observed	Silicoflagellate
ST31A	ESS	High diversity. Abundant *Chaetoceros, few Rhizosolenia, Thallasiosira, Bacterosira, Navicula*	None observed	
ST31B	ESS	High diversity. Few *Chaetoceros, Thallasiosira, Fragilariopsis*	Few *Protoperidinium*	
ST34	ESS	Abundant *Chaetoceros*, few *Thalassiosira, Navicula*	Few *Protoperidinium*	

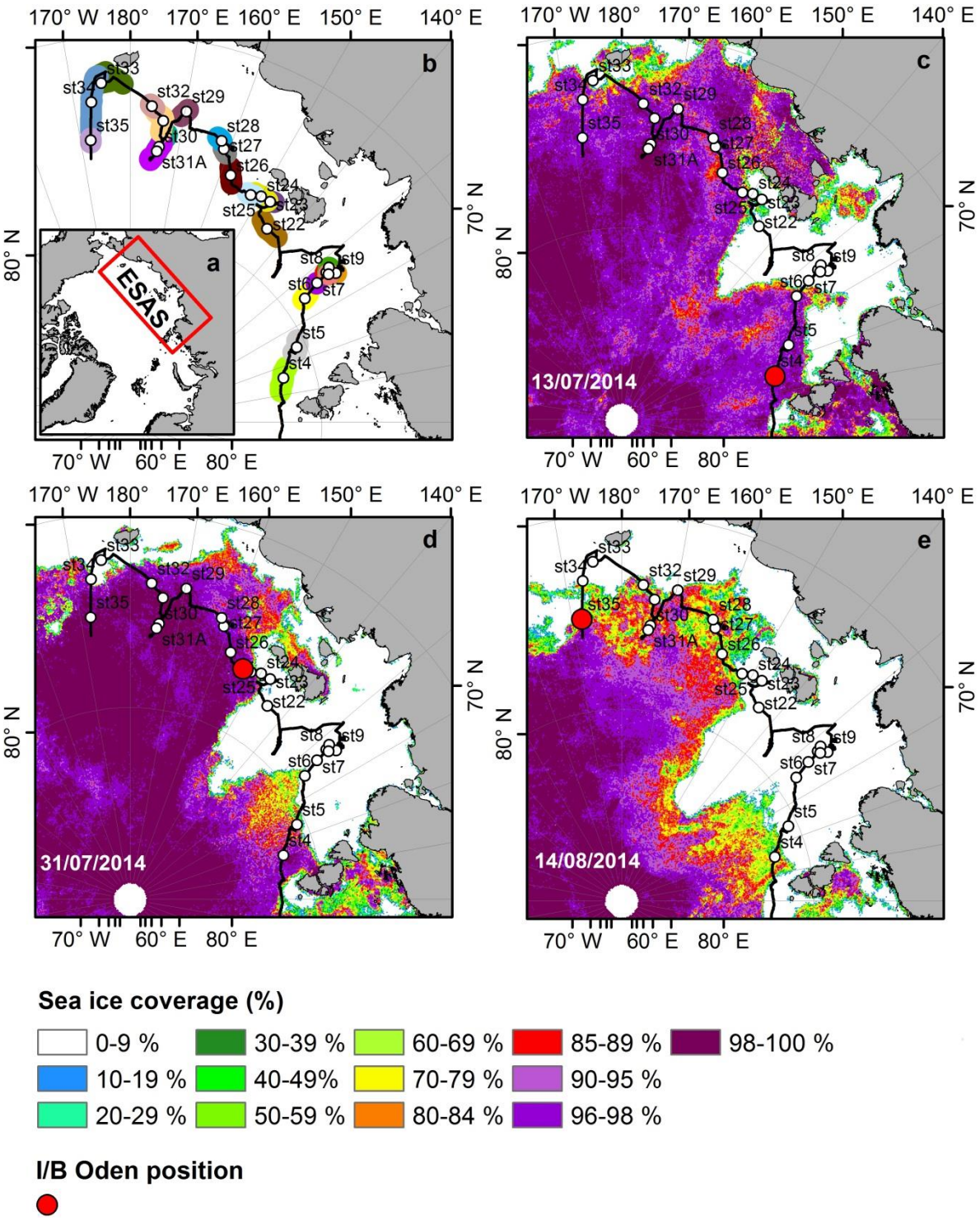

Fig. 1 (a) The study area in the East Siberian Arctic Shelf. (b) Time-averaged position during the large-volume filtration (circles) of the POM (>10μm) samples. Shaded coloured areas show the sampling area covered to harvest each POM (>10μm) sample. Sea-ice extent and concentration at the beginning (c), in the middle (d) and at the end (e) of the sampling campaign. The ship position is shown by a filled red circle.

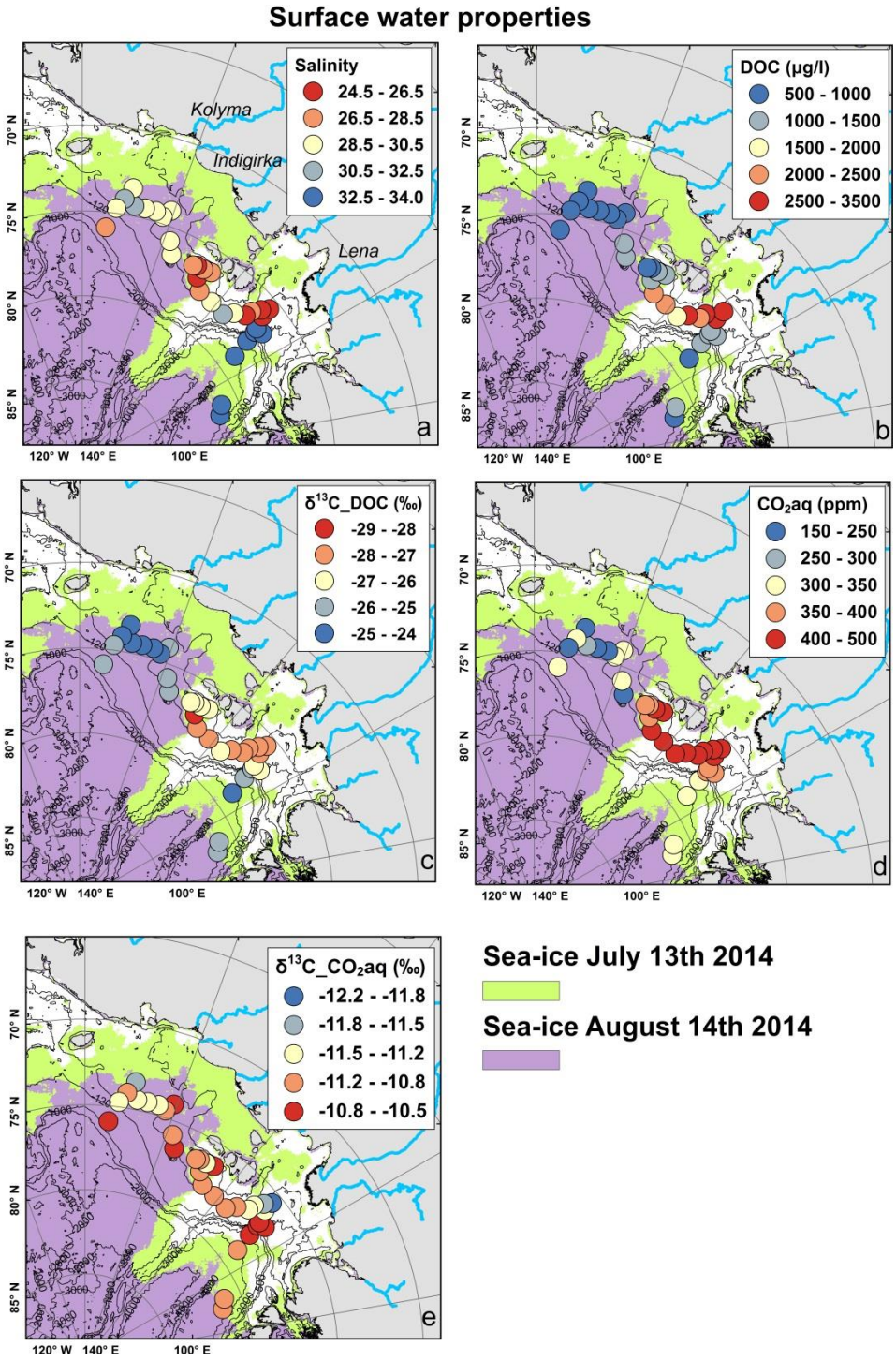

493

494

495 **Fig.2** Surface water properties. (a) Salinity. (b) DOC. (c) δ^{13}C-DOC. (d) CO_2aq. (e) δ^{13}C-

496 CO_2aq. Shaded areas show the sea-ice extent at the beginning (13/07/2014) and at the end of

497 the sampling campaign (14/08/2014) (Humborg et al., 2017; Salvadó et al., 2016).

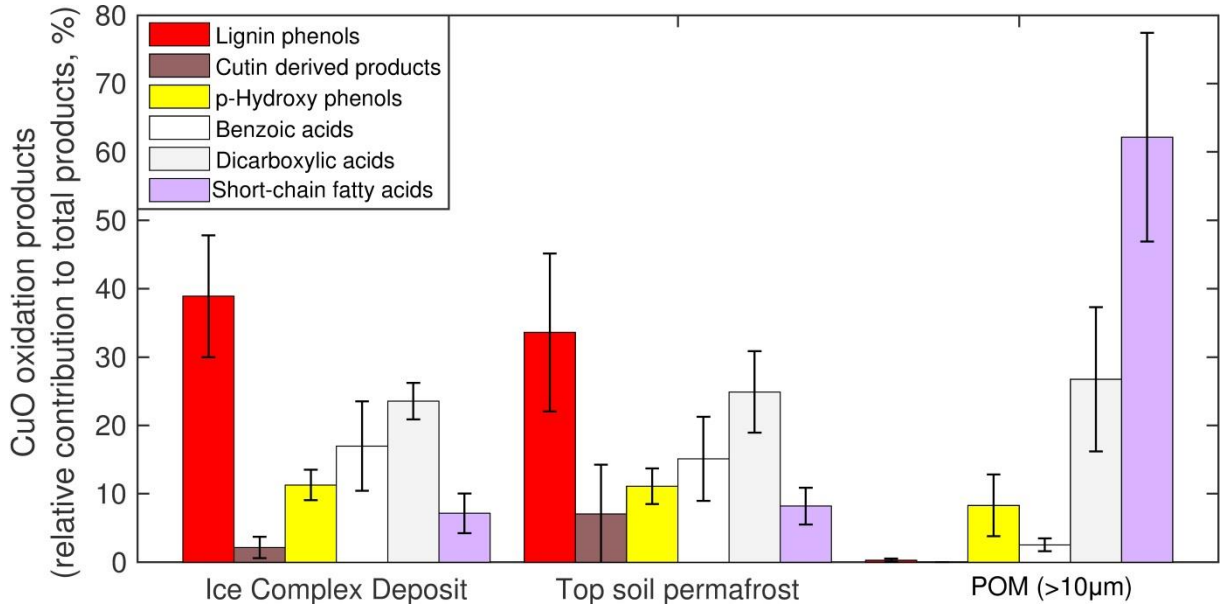

498

499

500

501

502 **Fig.3** Alkaline CuO fingerprint of top-soil permafrost samples (Tesi et al., 2014), Pleistocene
503 Ice Complex Deposit (Tesi et al., 2014) and POM (>10µm) fraction (this study). The plot
504 displays the relative proportion products yield upon alkaline CuO oxidation. The error bar
505 refers to the natural variability of each dataset

506

507

508

509

510

511

512

513

514

515

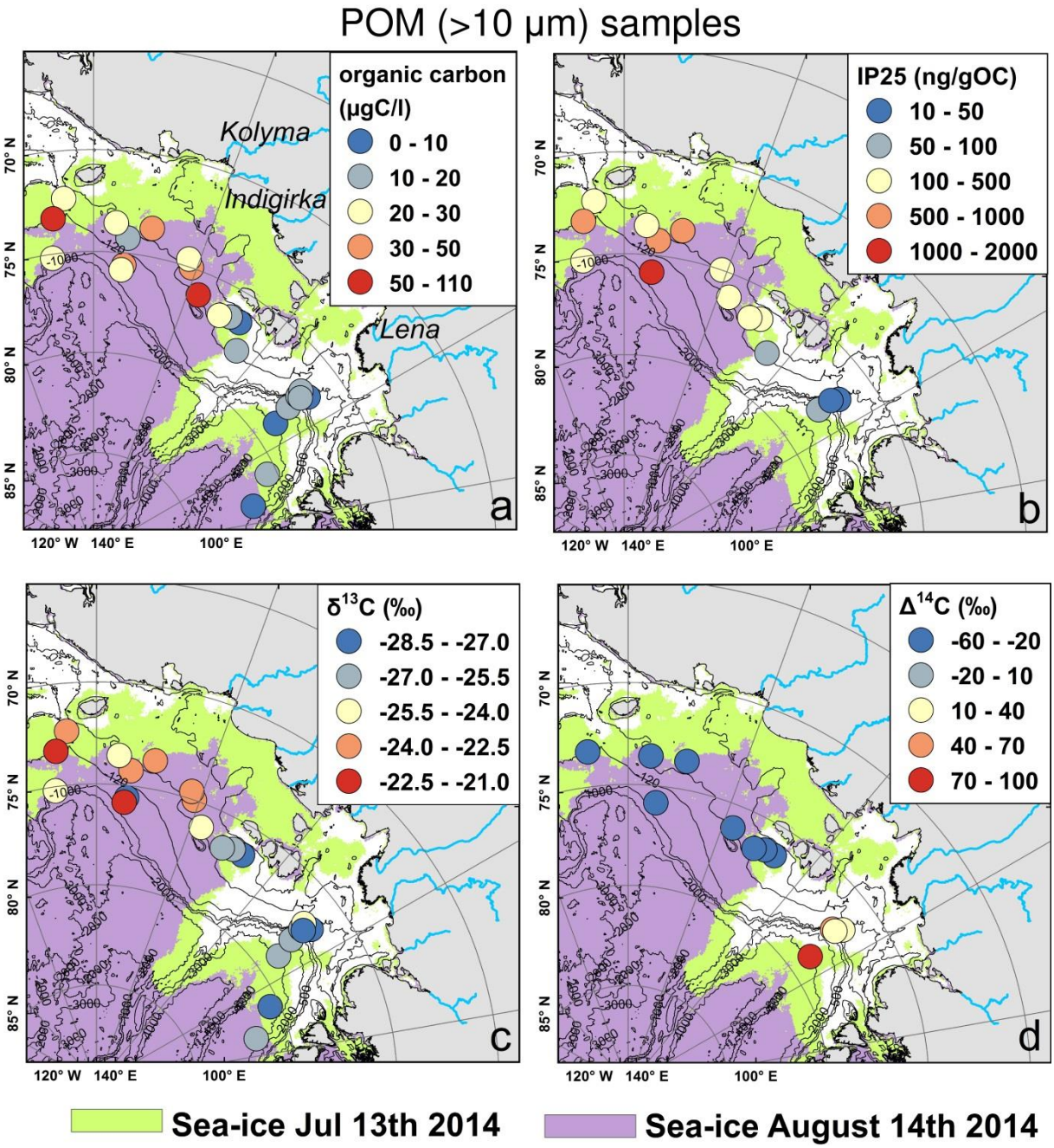

Fig. 4 POM (>10µm) composition (a) Organic carbon concentration. (b) IP25 (mono-unsaturated highly branched isoprenoid. (c) $\delta^{13}C$. (d) $\Delta^{14}C$. Shaded areas show the sea-ice extent at the beginning (13/07/2014) and at the end of the sampling campaign (14/08/2014).

524

525

526 **Fig. 5** SEM images. (a) ST-11: Dinoflagellates (*Protoperidinium* spp.) in open-waters of the
527 Laptev Sea. (b) ST22: Diatoms, mostly spines (setae) of *Chaetoceros* spp. in the transition
528 between Laptev Sea and East Siberian Sea. (c) ST-34: Diatoms from sea-ice dominated
529 waters in the East Siberian Sea

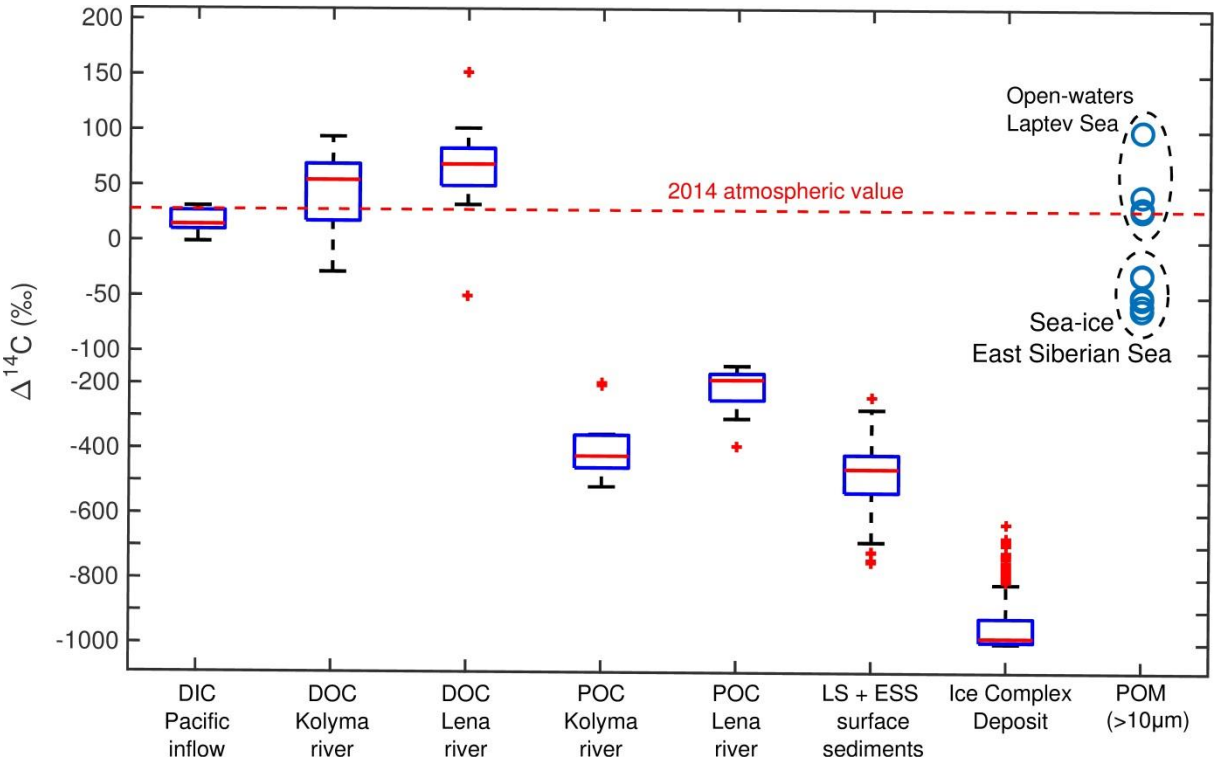

530

531

532

533 **Fig. 6** Radiocarbon signature of inorganic and organic carbon pools. Whisker plots of
534 radiocarbon values for different inorganic and organic carbon sources from the literature,
535 compared to the outer Laptev Sea and outer East Siberian Sea (blue circles, this study). Solid
536 lines show the median, the box limits display the 25th and 75th percentiles while the crosses
537 show the outliers. Source: DIC (Griffith et al., 2012), DOC-Kolyma (2009-2014), DOC-Lena
538 (2009-2014), POC-Kolyma (2009-2011), POC-Lena (2009-2011)
539 (www.arcticgreatrivers.org), Laptev Sea and Eastern Siberia Sea surface sediments (Salvadó
540 et al., 2016; Vonk et al., 2012) and Ice Complex Deposit (Vonk et al., 2012).

541

542

543

544

545

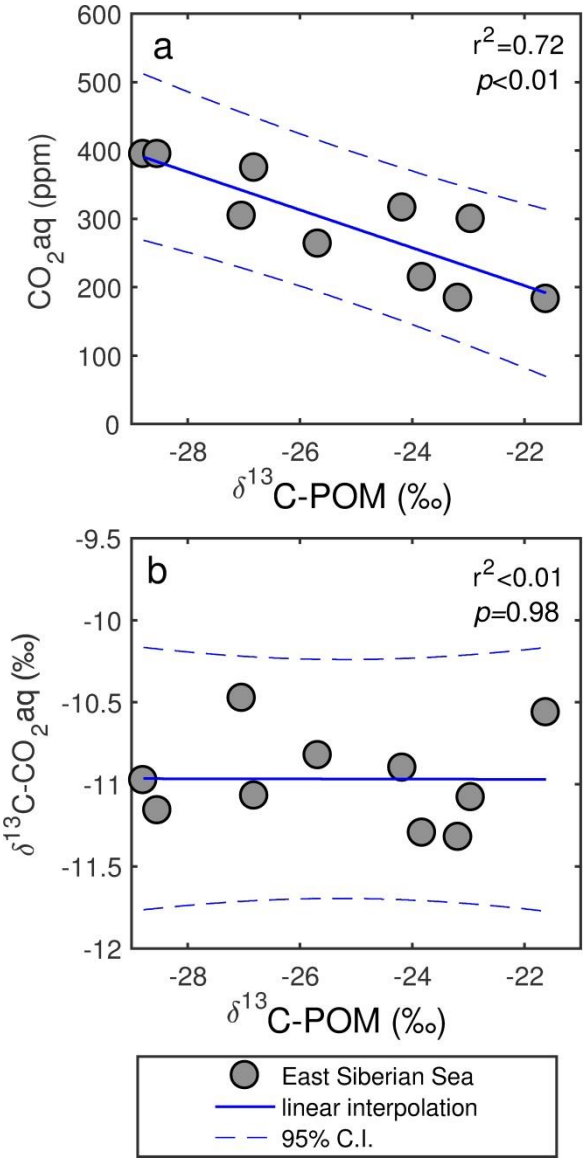

Fig. 7 Correlations (a) CO_2aq vs $\delta^{13}C$ (POM (>10μm) fraction) and (b) $\delta^{13}C$-CO_2aq vs $\delta^{13}C$ in the East Siberian Sea (filled circles). The solid line shows the linear interpolation while the dashed line shows the 95% confidence intervals.

References

Aagaard, K. and Carmack, E. C.: The role of sea ice and other fresh water in the Arctic circulation, Journal of Geophysical Research: Oceans, 94, 14485-14498, 1989.

Alling, V., Sanchez-Garcia, L., Porcelli, D., Pugach, S., Vonk, J. E., van Dongen, B., Mörth, C.-M., Anderson, L. G., Sokolov, A., Andersson, P., Humborg, C., Semiletov, I., and Gustafsson, Ö.: Nonconservative behavior of dissolved organic carbon across the Laptev and East Siberian seas, Global Biogeochemical Cycles, 24, n/a-n/a, 2010.

Amon, R., Rinehart, A., Duan, S., Louchouarn, P., Prokushkin, A., Guggenberger, G., Bauch, D., Stedmon, C., Raymond, P., and Holmes, R.: Dissolved organic matter sources in large Arctic rivers, Geochimica et Cosmochimica Acta, 94, 217-237, 2012.

Anderson, L. G., Björk, G., Jutterström, S., Pipko, I., Shakhova, N., Semiletov, I., and Wåhlström, I.: East Siberian Sea, an Arctic region of very high biogeochemical activity, Biogeosciences, 8, 1745-1754, 2011.

Anderson, L. G., Jutterström, S., Hjalmarsson, S., Wåhlström, I., and Semiletov, I.: Out-gassing of CO2 from Siberian Shelf seas by terrestrial organic matter decomposition, Geophysical Research Letters, 36, 2009.

Ardyna, M., Babin, M., Gosselin, M., Devred, E., Rainville, L., and Tremblay, J. É.: Recent Arctic Ocean sea ice loss triggers novel fall phytoplankton blooms, Geophysical Research Letters, 41, 6207-6212, 2014.

Arrigo, K. R., van Dijken, G., and Pabi, S.: Impact of a shrinking Arctic ice cover on marine primary production, Geophysical Research Letters, 35, n/a-n/a, 2008.

Belt, S. T., Brown, T. A., Rodriguez, A. N., Sanz, P. C., Tonkin, A., and Ingle, R.: A reproducible method for the extraction, identification and quantification of the Arctic sea ice proxy IP25 from marine sediments, Analytical Methods, 4, 705-713, 2012.

Belt, S. T., Massé, G., Rowland, S. J., Poulin, M., Michel, C., and LeBlanc, B.: A novel chemical fossil of palaeo sea ice: IP25, Organic Geochemistry, 38, 16-27, 2007.

Björk, G., Jutterström, S., Pipko, I., Shakhova, N., Semiletov, I., and Wåhlström, I.: East Siberian Sea, an Arctic region of very high biogeochemical activity, Biogeosciences, 8, 1745, 2011.

Bröder, L., Tesi, T., Andersson, A., Eglinton, T. I., Semiletov, I. P., Dudarev, O. V., Roos, P., and Gustafsson, Ö.: Historical records of organic matter supply and degradation status in the East Siberian Sea, Organic Geochemistry, 91, 16-30, 2016a.

Bröder, L., Tesi, T., Salvadó, J. A., Semiletov, I. P., Dudarev, O. V., and Gustafsson, Ö.: Fate of terrigenous organic matter across the Laptev Sea from the mouth of the Lena River to the deep sea of the Arctic interior, Biogeosciences, 13, 5003-5019, 2016b.

Brown, T. A., Belt, S. T., Tatarek, A., and Mundy, C. J.: Source identification of the Arctic sea ice proxy IP25, 5, 4197, 2014a.

Brown, T. A., Belt, S. T., Tatarek, A., and Mundy, C. J.: Source identification of the Arctic sea ice proxy IP25, Nature Communications, 5, 4197, 2014b.

Carlsson, P., Graneli, E., Tester, P., and Boni, L.: Influences of riverine humic substances on bacteria, protozoa, phytoplankton, and copepods in a coastal plankton community, Marine Ecology Progress Series, 127, 213-221, 1995.

Comiso, J. C., Parkinson, C. L., Gersten, R., and Stock, L.: Accelerated decline in the Arctic sea ice cover, Geophysical research letters, 35, 2008.

Dethleff, D.: Entrainment and export of Laptev Sea ice sediments, Siberian Arctic, Journal of Geophysical Research: Oceans, 110, n/a-n/a, 2005.

Ding, Q., Schweiger, A., Lheureux, M., Battisti, D. S., Po-Chedley, S., Johnson, N. C., Blanchard-Wrigglesworth, E., Harnos, K., Zhang, Q., Eastman, R., and Steig, E. J.: Influence of high-latitude atmospheric circulation changes on summertime Arctic sea ice, Nature Clim. Change, 7, 289-295, 2017.

605 Dittmar, T. and Kattner, G.: The biogeochemistry of the river and shelf ecosystem of the Arctic
606 Ocean: a review, Marine chemistry, 83, 103-120, 2003.
607 Dunton, K. H., Weingartner, T., and Carmack, E. C.: The nearshore western Beaufort Sea ecosystem:
608 Circulation and importance of terrestrial carbon in arctic coastal food webs, Progress in
609 Oceanography, 71, 362-378, 2006.
610 Feng, X., Gustafsson, Ö., Holmes, R. M., Vonk, J. E., van Dongen, B. E., Semiletov, I. P., Dudarev, O. V.,
611 Yunker, M. B., Macdonald, R. W., Wacker, L., Montluçon, D. B., and Eglinton, T. I.: Multimolecular
612 tracers of terrestrial carbon transfer across the pan-Arctic: 14C characteristics of sedimentary carbon
613 components and their environmental controls, Global Biogeochemical Cycles, 29, 1855-1873, 2015.
614 Fichot, C. G., Kaiser, K., Hooker, S. B., Amon, R. M., Babin, M., Bélanger, S., Walker, S. A., and Benner,
615 R.: Pan-Arctic distributions of continental runoff in the Arctic Ocean, Scientific reports, 3, 1053, 2013.
616 Frey, K. E. and Smith, L. C.: Amplified carbon release from vast West Siberian peatlands by 2100,
617 Geophysical Research Letters, 32, 2005.
618 Fujiwara, A., Hirawake, T., Suzuki, K., Imai, I., and Saitoh, S.-I.: Timing of sea ice retreat can alter
619 phytoplankton community structure in the western Arctic Ocean, Biogeosciences, 11, 1705-1716,
620 2014.
621 Gervais, F. and Riebesell, U.: Effect of phosphorus limitation on elemental composition and stable
622 carbon isotope fractionation in a marine diatom growing under different CO2 concentrations,
623 Limnology and Oceanography, 46, 497-504, 2001.
624 Goñi, M. A. and Hedges, J. I.: Potential applications of cutin-derived CuO reaction products for
625 discriminating vascular plant sources in natural environments, Geochimica et Cosmochimica Acta, 54,
626 3073-3081, 1990.
627 Goñi, M. A. and Hedges, J. I.: Sources and reactivities of marine-derived organic matter in coastal
628 sediments as determined by alkaline CuO oxidation, Geochimica et Cosmochimica Acta, 59, 2965-
629 2981, 1995.
630 Gordeev, V. V.: Fluvial sediment flux to the Arctic Ocean, Geomorphology, 80, 94-104, 2006.
631 Griffith, D. R., McNichol, A. P., Xu, L., McLaughlin, F. A., Macdonald, R. W., Brown, K. A., and Eglinton,
632 T. I.: Carbon dynamics in the western Arctic Ocean: insights from full-depth carbon isotope profiles of
633 DIC, DOC, and POC, 2012. 2012.
634 Gustafsson, Ö., Andersson, P., Axelman, J., Bucheli, T., Kömp, P., McLachlan, M., Sobek, A., and
635 Thörngren, J.-O.: Observations of the PCB distribution within and in-between ice, snow, ice-rafted
636 debris, ice-interstitial water, and seawater in the Barents Sea marginal ice zone and the North Pole
637 area, Science of the total environment, 342, 261-279, 2005.
638 Gustafsson, Ö. and Andersson, P. S.: 234Th-derived surface export fluxes of POC from the Northern
639 Barents Sea and the Eurasian sector of the Central Arctic Ocean, Deep Sea Research Part I:
640 Oceanographic Research Papers, 68, 1-11, 2012.
641 Hoins, M., Van de Waal, D. B., Eberlein, T., Reichart, G.-J., Rost, B., and Sluijs, A.: Stable carbon
642 isotope fractionation of organic cyst-forming dinoflagellates: Evaluating the potential for a CO2
643 proxy, Geochimica et Cosmochimica Acta, 160, 267-276, 2015.
644 Humborg, C., Geibel, M. C., Anderson, L. G., Björk, G., Mörth, C.-M., Sundbom, M., Thornton, B. F.,
645 Deutsch, B., Gustafsson, E., Gustafsson, B., Ek, J., and Semiletov, I.: Sea-air exchange patterns along
646 the central and outer East Siberian Arctic Shelf as inferred from continuous CO2, stable isotope and
647 bulk chemistry measurements Global Biogeochemical Cycles, doi: 10.1002/2017GB005656, 2017.
648 2017.
649 Iken, K., Bluhm, B., and Gradinger, R.: Food web structure in the high Arctic Canada Basin: evidence
650 from δ13C and δ15N analysis, Polar Biology, 28, 238-249, 2005.
651 Janout, M. A., Hölemann, J., Waite, A. M., Krumpen, T., Appen, W. J., and Martynov, F.: Sea-ice
652 retreat controls timing of summer plankton blooms in the Eastern Arctic Ocean, Geophysical
653 Research Letters, 2016. 2016.
654 Karlsson, E., Gelting, J., Tesi, T., Dongen, B., Andersson, A., Semiletov, I., Charkin, A., Dudarev, O., and
655 Gustafsson, Ö.: Different sources and degradation state of dissolved, particulate and sedimentary
656 organic matter along the Eurasian Arctic coastal margin, Global Biogeochemical Cycles, 2016. 2016.

Kohlbach, D., Graeve, M., A Lange, B., David, C., Peeken, I., and Flores, H.: The importance of ice algae-produced carbon in the central Arctic Ocean ecosystem: Food web relationships revealed by lipid and stable isotope analyses, Limnology and Oceanography, 2016. 2016.

Kwok, R. and Rothrock, D.: Decline in Arctic sea ice thickness from submarine and ICESat records: 1958–2008, Geophysical Research Letters, 36, 2009.

Lalande, C., Bélanger, S., and Fortier, L.: Impact of a decreasing sea ice cover on the vertical export of particulate organic carbon in the northern Laptev Sea, Siberian Arctic Ocean, Geophysical Research Letters, 36, n/a-n/a, 2009.

Lalande, C., Nöthig, E. M., Somavilla, R., Bauerfeind, E., Shevchenko, V., and Okolodkov, Y.: Variability in under-ice export fluxes of biogenic matter in the Arctic Ocean, Global Biogeochemical Cycles, 28, 571-583, 2014.

Lantuit, H., Atkinson, D., Paul Overduin, P., Grigoriev, M., Rachold, V., Grosse, G., and Hubberten, H.-W.: Coastal erosion dynamics on the permafrost-dominated Bykovsky Peninsula, north Siberia, 1951–2006, Polar Research, 30, 7341, 2011.

Laws, E. A., Bidigare, R. R., and Popp, B. N.: Effect of growth rate and CO~ 2 concentration on carbon isotopic fractionation by the marine diatom Phaeodactylum tricornutum, Limnology and Oceanography, 42, 1552-1560, 1997a.

Laws, E. A., Bidigare, R. R., and Popp, B. N.: Effect of growth rate and CO~ 2 concentration on carbon isotopic fractionation by the marine diatom Phaeodactylum tricornutum, 1997b. 1997b.

Laws, E. A., Popp, B. N., Bidigare, R. R., Kennicutt, M. C., and Macko, S. A.: Dependence of phytoplankton carbon isotopic composition on growth rate and [CO2) aq: Theoretical considerations and experimental results, Geochimica et cosmochimica acta, 59, 1131-1138, 1995.

McClelland, J. W., Holmes, R. M., Peterson, B. J., Raymond, P. A., Striegl, R., Zhulidov, A. V., Zimov, S., Zimov, N., Tank, S. E., and Spencer, R. G.: Particulate organic carbon and nitrogen export from major Arctic rivers, Global Biogeochemical Cycles, 30, 629-643, 2016.

Nieuwenhuize, J., Maas, Y. E., and Middelburg, J. J.: Rapid analysis of organic carbon and nitrogen in particulate materials, Marine Chemistry, 45, 217-224, 1994.

Pagani, M., Arthur, M. A., and Freeman, K. H.: Miocene evolution of atmospheric carbon dioxide, Paleoceanography, 14, 273-292, 1999.

Pipko, I. I., Pugach, S. P., and Semiletov, I. P.: The autumn distribution of the CO2 partial pressure in bottom waters of the East Siberian Sea, Doklady Earth Sciences, 425, 345-349, 2009.

Popp, B. N., Laws, E. A., Bidigare, R. R., Dore, J. E., Hanson, K. L., and Wakeham, S. G.: Effect of phytoplankton cell geometry on carbon isotopic fractionation, Geochimica et cosmochimica acta, 62, 69-77, 1998.

Popp, B. N., Trull, T., Kenig, F., Wakeham, S. G., Rust, T. M., Tilbrook, B., Griffiths, B., Wright, S. W., Marchant, H. J., and Bidigare, R. R.: Controls on the carbon isotopic composition of Southern Ocean phytoplankton, Global Biogeochemical Cycles, 13, 827-843, 1999.

Purina, I., Balode, M., Béchemin, C., Põder, T., Vérité, C., and Maestrini, S.: Influence of dissolved organic matter from terrestrial origin on the changes of dinoflagellate species composition in the Gulf of Riga, Baltic Sea, Hydrobiologia, 514, 127-137, 2004.

Rau, G., Riebesell, U., and Wolf-Gladrow, D.: A model of photosynthetic 13C fractionation by marine phytoplankton based on diffusive molecular CO2 uptake, Marine Ecology Progress Series, 133, 275-285, 1996.

Rau, G. H.: Variations in sedimentary organic δ13C as a proxy for past changes in ocean and atmospheric CO2 concentrations. In: Carbon Cycling in the Glacial Ocean: Constraints on the Ocean's Role in Global Change, Springer, 1994.

Salvadó, J. A., Tesi, T., Sundbom, M., Karlsson, E., Kruså, M., Semiletov, I. P., Panova, E., and Gustafsson, Ö.: Contrasting composition of terrigenous organic matter in the dissolved, particulate and sedimentary organic carbon pools on the outer East Siberian Arctic Shelf, Biogeosciences, 13, 6121-6138, 2016.

Sánchez-García, L., Alling, V., Pugach, S., Vonk, J., van Dongen, B., Humborg, C., Dudarev, O., Semiletov, I., and Gustafsson, Ö.: Inventories and behavior of particulate organic carbon in the Laptev and East Siberian seas, Global Biogeochemical Cycles, 25, 2011.
Semiletov, I., Dudarev, O., Luchin, V., Charkin, A., Shin, K. H., and Tanaka, N.: The East Siberian Sea as a transition zone between Pacific-derived waters and Arctic shelf waters, Geophysical Research Letters, 32, 2005.
Semiletov, I., Pipko, I., Gustafsson, O., Anderson, L. G., Sergienko, V., Pugach, S., Dudarev, O., Charkin, A., Gukov, A., Broder, L., Andersson, A., Spivak, E., and Shakhova, N.: Acidification of East Siberian Arctic Shelf waters through addition of freshwater and terrestrial carbon, Nature Geosci, 9, 361-365, 2016.
Semiletov, I. P., Shakhova, N. E., Pipko, I. I., Pugach, S. P., Charkin, A. N., Dudarev, O. V., Kosmach, D. A., and Nishino, S.: Space-time dynamics of carbon and environmental parameters related to carbon dioxide emissions in the Buor-Khaya Bay and adjacent part of the Laptev Sea, Biogeosciences, 10, 5977, 2013.
Sobek, A. and Gustafsson, Ö.: Latitudinal fractionation of polychlorinated biphenyls in surface seawater along a 62 N− 89 N transect from the southern Norwegian Sea to the North Pole area, Environmental science & technology, 38, 2746-2751, 2004.
Spreen, G., Kaleschke, L., and Heygster, G.: Sea ice remote sensing using AMSR-E 89-GHz channels, Journal of Geophysical Research: Oceans, 113, 2008.
Tesi, T., Muschitiello, F., Smittenberg, R. H., Jakobsson, M., Vonk, J. E., Hill, P., Andersson, A., Kirchner, N., Noormets, R., Dudarev, O., Semiletov, I., and Gustafsson, Ö.: Massive remobilization of permafrost carbon during post-glacial warming, Nature Communications, 7, 13653, 2016.
Tesi, T., Puig, P., Palanques, A., and Goñi, M.: Lateral advection of organic matter in cascading-dominated submarine canyons, Progress in Oceanography, 84, 185-203, 2010.
Tesi, T., Semiletov, I., Hugelius, G., Dudarev, O., Kuhry, P., and Gustafsson, Ö.: Composition and fate of terrigenous organic matter along the Arctic land–ocean continuum in East Siberia: Insights from biomarkers and carbon isotopes, Geochimica et Cosmochimica Acta, 133, 235-256, 2014.
Torres-Valdés, S., Tsubouchi, T., Bacon, S., Naveira-Garabato, A. C., Sanders, R., McLaughlin, F. A., Petrie, B., Kattner, G., Azetsu-Scott, K., and Whitledge, T. E.: Export of nutrients from the Arctic Ocean, Journal of Geophysical Research: Oceans, 118, 1625-1644, 2013.
Vonk, J., Sánchez-García, L., Van Dongen, B., Alling, V., Kosmach, D., Charkin, A., Semiletov, I. P., Dudarev, O. V., Shakhova, N., and Roos, P.: Activation of old carbon by erosion of coastal and subsea permafrost in Arctic Siberia, Nature, 489, 137-140, 2012.
Vonk, J. E., Semiletov, I. P., Dudarev, O. V., Eglinton, T. I., Andersson, A., Shakhova, N., Charkin, A., Heim, B., and Gustafsson, Ö.: Preferential burial of permafrost-derived organic carbon in Siberian-Arctic shelf waters, Journal of Geophysical Research: Oceans, 119, 8410-8421, 2014.
Wegner, C., Hölemann, J. A., Dmitrenko, I., Kirillov, S., Tuschling, K., Abramova, E., and Kassens, H.: Suspended particulate matter on the Laptev Sea shelf (Siberian Arctic) during ice-free conditions, Estuarine, Coastal and Shelf Science, 57, 55-64, 2003.
Wikner, J. and Andersson, A.: Increased freshwater discharge shifts the trophic balance in the coastal zone of the northern Baltic Sea, Global Change Biology, 18, 2509-2519, 2012.
Wolf-Gladrow, D. A., Riebesell, U., Burkhardt, S., and Bijma, J.: Direct effects of CO2 concentration on growth and isotopic composition of marine plankton, Tellus B, 51, 461-476, 1999.